GaAsP/InGaP heterojunction bipolar transistors grown by MOCVD

GaAsP/InGaP Heterojunction Bipolar Transistors Grown by MOCVD

Christopher Heidelberger[1] and Eugene A. Fitzgerald

Department of Materials Science and Engineering, Massachusetts Institute of Technology, Cambridge, MA 02139, USA

[1]Corresponding Author: Phone: 617-253-6903, Email: chrish@mit.edu

Abstract

Heterojunction bipolar transistors with $GaAs_xP_{1-x}$ bases and collectors and $In_yGa_{1-y}P$ emitters were grown on GaAs substrates via metalorganic chemical vapor deposition (MOCVD), fabricated using conventional techniques, and electrically tested. Four different $GaAs_xP_{1-x}$ compositions were used, ranging from $x = 0.825$ to $x = 1$ (GaAs), while the $In_yGa_{1-y}P$ composition was adjusted to remain lattice-matched to the GaAsP. DC current gain close to or exceeding 100 is measured for 60 μm diameter devices of all compositions. Physical mechanisms governing base current and therefore current gain are investigated. The collector current is determined not to be affected by the barrier caused by the conduction band offset between the InGaP emitter and GaAsP base. While the collector current for the GaAs/InGaP devices is well-predicted by diffusion of electrons across the quasi-neutral base, the collector current of the GaAsP/InGaP devices exceeds this estimate by an order of magnitude. This results in higher transconductance for GaAsP/InGaP than would be estimated from known materials properties.

1 Introduction

GaAs/InGaP HBTs have been widely studied and have found several commercial applications, including in power amplifiers for mobile phone handsets.[1] They hold an advantage over similar GaAs/AlGaAs HBTs because of the lower conduction band offset and higher valence band offset of the GaAs/InGaP heterojunction, resulting in improved collection efficiency.[2,3] In addition, they avoid oxygen-related defects associated with AlGaAs layers and have superior wet-etching selectivity to GaAs/AlGaAs heterostructures.

$GaAs_xP_{1-x}$ with $0.8 < x < 1$ can be substituted for GaAs in the base and collector layers, while still using an $In_yGa_{1-y}P$ emitter with y adjusted to keep the emitter lattice-matched to the base and collector. At these compositions of GaAsP, there is not a significant decrease in electron mobility from GaAs.[4] The use of GaAsP instead of GaAs offers several advantages. The higher band gap of GaAsP allows for higher breakdown voltage. In addition, there has been recent interest in monolithic integration of III-V transistors with Si CMOS circuitry.[5–7] With decreasing As content, the lattice constant of GaAsP decreases, getting closer to that of Si. The reduced lattice mismatch simplifies growth of III-V device layers with sufficiently low defect density. Lastly, the coefficient of thermal expansion (CTE) of GaAsP is lower than that of GaAs and closer to that of Si, reducing the likelihood of the III-V epi-layers cracking due to CTE mismatch between the films and the substrate.[8]

In this work, we demonstrate GaAsP/InGaP transistors at a range of compositions from x = 0.825 to x = 1 (GaAs). These devices are grown on GaAs substrates rather than Si substrates. This is to decouple the effect of GaAsP composition from that of any defects formed due to the high lattice mismatch between the device layers and Si as well as from the III-V on group IV interface.

2 Experimental

2.1 MOCVD Growth

All epitaxial structures were grown in a Thomas Swan/Aixtron cold-walled 6x2" metalorganic chemical vapor deposition (MOCVD) reactor with a close-coupled showerhead configuration. Trimethylgallium (TMGa), trimethylindium (TMIn), AsH_3, PH_3, Si_2H_6, and $CBrCl_3$ were used as precursors. The total reactor pressure for all samples was 100 Torr and N_2 was used as a carrier gas. The susceptor rotation speed was 100 rpm. Growth rates were approximately 0.55 nm/s for GaAs and GaAsP and 0.35 nm/s for InGaP.

Four HBT structures were grown with $GaAs_xP_{1-x}$ compositions of x = 0.825, 0.873, 0.941, and 1. Table 1 shows the generalized epitaxial structure. All samples were grown on n+ (100) GaAs substrates, with a 6° offcut towards the nearest <111>B direction. This particular offcut was chosen because GaAsP or GaAs grown at temperatures above 600 °C on (100) SiGe or Ge, respectively, with a 6° offcut towards the nearest <111> direction will adopt this orientation.[9] A tensile $GaAs_xP_{1-x}$ compositionally graded buffer was used to reach the desired lattice constant for the final device layers. A compositional grade rate of 0.2% strain/μm was used, resulting in buffer thicknesses varying from 0 nm (x = 1) to 4 μm (x = 0.825). This low rate was chosen to avoid formation of cracks or so-called "faceted trenches" due to the tensile strain, rather than strain relaxation through plastic deformation.[10,11] The $In_yGa_{1-y}P$ emitter layer was grown with a composition lattice-matched to the GaAsP layers directly above and below. A 5 s purge step, holding group V precursor flow rates constant from the previous layer, was implemented while switching from GaAsP to InGaP and from InGaP to GaAsP. The graded buffers were grown with a substrate temperature of 725 °C to increase dislocation glide velocities and therefore relaxation of the films.[12] Device layers were then grown at 650 °C, except for the GaAsP base

layer, which was grown at 600 °C to increase the incorporation of the C dopant.[13] All temperature ramps were executed with a group V overpressure (mixed AsH_3 and PH_3) but with no group III precursor flow.

2.2 Film Characterization

Lattice constant of the films—and by Vegard's law, their composition—were measured using high-resolution x-ray diffraction (XRD) using a procedure described previously.[13] Film thicknesses and morphologies were verified using cross-section transmission electron microscopy (TEM) with an accelerating voltage of 200 kV. Electron-beam-induced current (EBIC) images were taken of the base-collector diode in the sample with x = 0.825. For this measurement, the upper contact and emitter layers were etched away. An accelerating voltage of 20 kV and beam current of 0.34 nA was used. This was used to measure the low threading dislocation density (TDD) in the GaAsP HBT device layers. Photoluminescence (PL) of the GaAsP films was measured using a 514.5 nm laser, a Si photodetector, and standard lock-in techniques. Dopant concentration of a representative sample was verified using secondary ion mass spectrometry (SIMS), performed by Evans Analytical Group.

2.3 HBT Fabrication and Testing

The HBTs were fabricated with concentric circular emitter and base mesas. A schematic cross-section of the finished devices is shown in Figure 1. The emitter mesa diameters, which define the size of the emitter-base junction, range from 15 µm to 240 µm. The emitter mesa was etched using a two-step process. First, the GaAsP contact layer was removed using H_2SO_4:H_2O_2:H_2O = 1:1:10; then, the InGaP emitter was removed using HCl:H_3PO_4 = 1:1. The H_2SO_4 etchant has been shown to not etch InGaP and the HCl etchant not to etch GaAs.[14,15] Even with x = 0.825, the HCl etchant is still highly selective against $GaAs_xP_{1-x}$ and therefore

does not etch into the base region. The base/collector mesa was then patterned using the H_2SO_4 etchant, timed to stop in the subcollector layer. The samples were dipped in H_2SO_4:H_2O = 1:10 for 60 s to remove any native oxide and then a 10 nm Al_2O_3 passivation layer was immediately deposited by atomic layer deposition (ALD). The Al_2O_3 was removed with 7:1 buffered oxide etch in the areas underneath the contacts before metal deposition. Non-alloyed emitter, base, and collector contacts were all deposited simultaneously by e-beam evaporation of Ti/Pt/Au (5 nm/40 nm/120 nm) and patterned by lift-off. Devices were electrically tested at 300 K using an Agilent B1500 semiconductor parameter analyzer.

Table 1: Epitaxial layer structure. Four samples were grown with x = 0.825, 0.873, 0.941, and 1. y was chosen such that the InGaP layer is lattice-matched to the surrounding GaAsP layers.

Layer	**Material**	**Thickness (nm)**	**Growth Temperature (°C)**	**Polarity**	**Doping (cm^{-3})**
Contact	$GaAs_xP_{1-x}$	100	650	*n*	2×10^{19} Si
Emitter Cap	$In_yGa_{1-y}P$	25	650	*n*	1×10^{18} Si
Emitter	$In_yGa_{1-y}P$	50	650	*n*	6×10^{17} Si
Spacer	$GaAs_xP_{1-x}$	3	650	*n*	UID
Base	$GaAs_xP_{1-x}$	90	600	*p*	7×10^{17} C
Collector	$GaAs_xP_{1-x}$	500	650	*n*	1×10^{17} Si
Sub-collector	$GaAs_xP_{1-x}$	500	650	*n*	5×10^{18} Si
Graded Buffer	ΔGaAsP	0–4000 (depending on final composition)	725	*n*	5×10^{18} Si
Initiation	GaAs	100	725	*n*	5×10^{18} Si
Substrate	GaAs	-	-	*n*	2×10^{18} Si

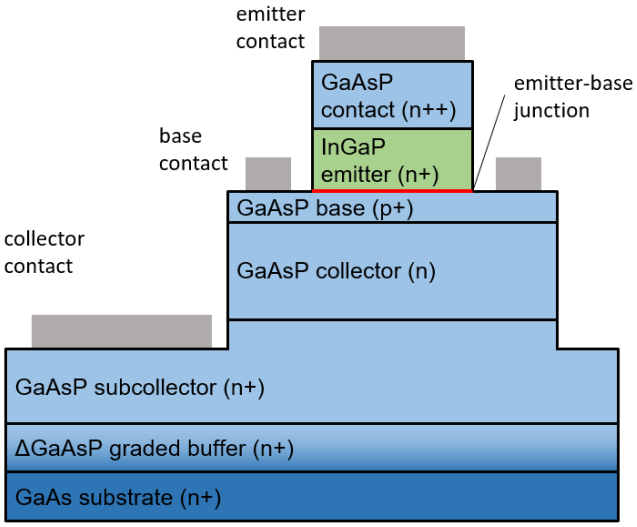

Figure 1: Cross-sectional schematic of GaAsP/InGaP HBT.

3 Results and Discussion

3.1 Epitaxial Film Characterization

XRD was performed on each sample to measure the GaAsP lattice constant and composition. The compositions measured by XRD are those listed in Section 2.1. The GaAsP device layers are nearly fully relaxed, with a maximum residual strain of 0.06%.

PL spectra from the GaAsP base/collector layers are shown in Figure 2. Band gap (E_g) for each sample was calculated by shifting the corresponding photon energy for each peak by −7 meV, the amount necessary for the GaAs peak to coincide with 1.424 eV. This shift can be attributed to electron-hole pairs recombining with non-zero momentum. E_g values from the GaAsP samples correspond well with what would be predicted by the XRD composition data, varying by less than 10 meV.[16]

Figure 3a shows a cross-section TEM image of the sample with x = 0.825. While misfit dislocations are visible in the GaAsP graded buffer region (not shown), there are no defects

visible in the active device layers. The InGaP/GaAsP emitter-base interface is sharp. Figure 3b shows a transmission electron diffraction (TED) pattern from the InGaP emitter along the (110) orientation. The superspots indicate the presence of Cu-Pt ordering.

Figure 4 shows an EBIC image of the base-collector diode of the structure with x = 0.825 (upper contact and emitter layers etched off). Threading dislocations originating in the GaAsP graded buffer layer extend to the surface of the sample, passing through the base-collector junction. The minority carrier lifetime is suppressed near these dislocations, resulting in a reduction in collected current and a dark spot in the EBIC image. The TDD in this sample is (1.5 ± 0.4) × 10^5 cm^{-2}. This dislocation density only has a small effect on the electron minority carrier lifetime in GaAs, such that current gain in an HBT with a narrow base width should not be affected.[17] The other samples with x > 0.825 have less lattice mismatch with the GaAs substrate. Therefore, this is likely an upper bound of the TDD for all of the samples discussed here.

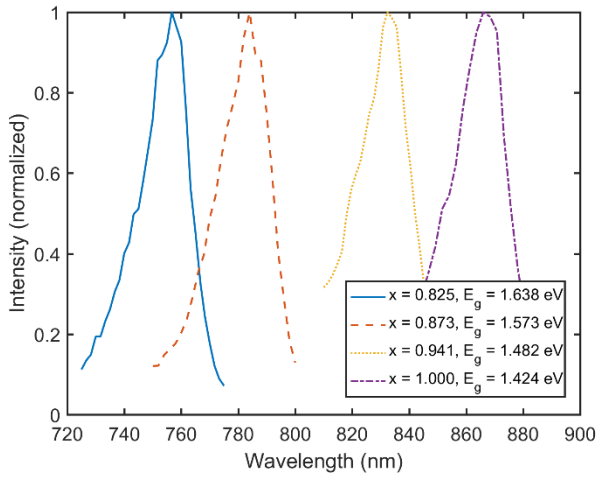

Figure 2: Photoluminescence spectra from the GaAsP base/collector layers.

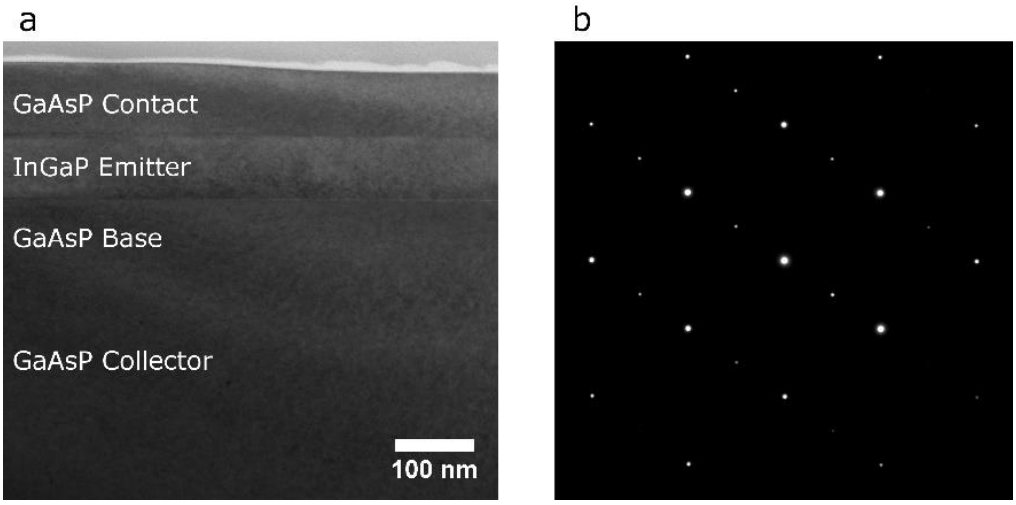

Figure 3: (a) Cross-section TEM image of GaAsP/InGaP HBT with x = 0.825 (Acc. Voltage = 200 kV). (b) (110) TED pattern from InGaP emitter area with superspots indicating Cu-Pt ordering.

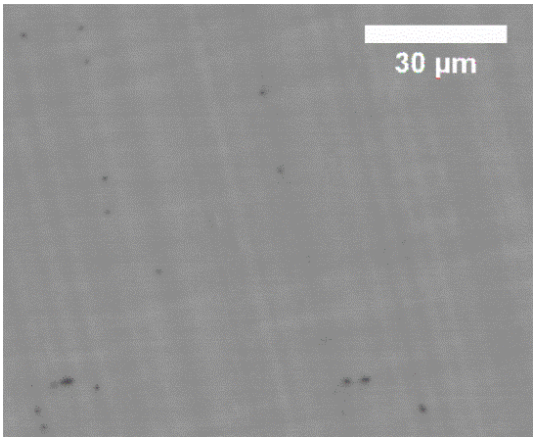

Figure 4: EBIC image of base-collector junction of the $GaAs_{0.825}P$ device under 0 V bias. Black spots are caused by recombination at threading dislocations originating from the underlying GaAsP graded buffer.

3.2 HBT DC Characteristics

Figure 5 shows Gummel plots—collector current (I_C) and base current (I_B) plotted as a function of the base-emitter voltage (V_{BE})—for the $GaAs_xP_{1-x}/In_yGa_{1-y}P$ HBTs of four different compositions (x = 1, 0.941, 0.873, 0.825). The diameter of the emitter-base junction (d, highlighted in Figure 1) is 60 µm and the base-collector voltage (V_{BC}) is 0 V. The ideality factor (n) of the collector current is close to 1 for all GaAsP compositions, ranging from 1.02 to 1.08.

I_B has two exponential regimes: $n \approx 1.8$ for I_B less than 10^{-9} A and $n \approx 1.4$ for I_B greater than 10^{-9} A.

Roll-off of both I_C and I_B at high V_{BE} is caused by series resistance at the emitter ohmic contact. This series resistance worsens as x decreases because of the increased band gap of the $GaAs_xP_{1-x}$ emitter contact layer. This could be mitigated by adding a mismatched n++ GaAs or InGaAs contact layer to all of the devices. In addition, contact resistance could be improved by using a separate alloyed Ge/Ni/Au contact to the n-type emitter and collector.[18]

Figure 6a shows I_C and I_B for a range of device sizes at V_{BE} = 0.930 V and V_{BC} = 0 V. At this biasing condition, I_C scales with area (d^2), indicating that the entire emitter-base junction is uniformly injecting electrons into the base. The collector current density (J_C) for all device sizes is 8×10^{-5} A·cm^{-2}. There are two different dependences of I_B on device diameter. For diameters smaller than 60 µm, I_B scales with $d^{1.3}$, while for those larger than 60 µm, it scales with d^2. Figure 6b shows the same as Figure 6a but at V_{BE} = 1.134 V and J_C = 0.13 A·cm^{-2}. At this current density, both I_C and I_B scale with d^2 across the entire range of device sizes.

A DC current gain (β) of over 100 was measured for all GaAsP compositions at relatively high collector current densities (J_C), greater than about 20 A·cm^{-2}. The only exception was the device with x = 0.825, where J_C could not reach this value due to series resistance and β only reached 60. However, β is reduced at lower current densities. The main sources of I_B—which limit β at lower current densities—can be ascertained by observing how I_B varies with active layer composition, with V_{BE}, and with emitter-base junction area (A_E).

For a given I_C, β does not change appreciably with GaAsP composition. With decreasing x, the valence band offset between $GaAs_xP_{1-x}$ and lattice-matched InGaP is expected to decrease.[19]

This indicates that backwards injection of holes from the base into the emitter does not contribute significantly to I_B, because this injection current would increase exponentially with decreasing valence band offset, thereby reducing β.

At smaller device sizes (d < 60 μm) and the lower current densities shown in Figure 6a, I_B is dominated by a process occurring at the perimeter of the emitter-base junction. Because I_B varies exponentially with V_{BE} in this regime with n close to 2 (Figure 5), we can conclude that it is likely space-charge region (SCR) recombination at the emitter-base interface occurring close to the perimeter of the device. This could be due to imperfect sidewall passivation near the emitter-base interface, or defects in the emitter base interface formed near the perimeter of the mesa during device processing. To improve performance at small device sizes, particularly for those smaller than what was fabricated for this study, it will be critical to identify and address this source of I_B.

At larger device sizes and larger currents, I_B is proportional to the area of the emitter-base junction (Figures 6a and 6b). $n \approx 1.4$ in this regime for all GaAsP compositions (Figure 5), which indicates a combination of SCR recombination and quasi-neutral region (QNR) recombination during electron transit across the base. The fact that SCR recombination still occurs even though no defects are visible in cross-section TEM of the emitter-base interface suggests that DC characteristics of GaAsP/InGaP HBTs are a more sensitive measure of interface quality than TEM of the GaAsP/InGaP interface. The GaAs/InGaP devices (x = 1) exhibit similar I_B behavior as the x = 0.825 devices shown in Figures 6a and 6b. This is further evidence that the recombination mechanisms governing I_B are not related to dislocations, but rather to interfacial defects between the InGaP emitter and GaAs(P) base. Future work may involve optimization of the growth conditions of this interface to reduce the rate of SCR.

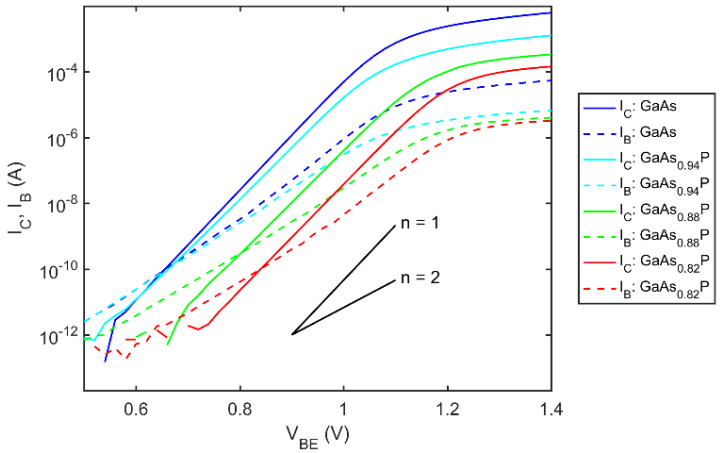

Figure 5: Gummel plots (collector current and base current vs emitter-base voltage) for GaAsP/InGaP HBTs of four different compositions. Measurement was taken with V_{BC} = 0 V.

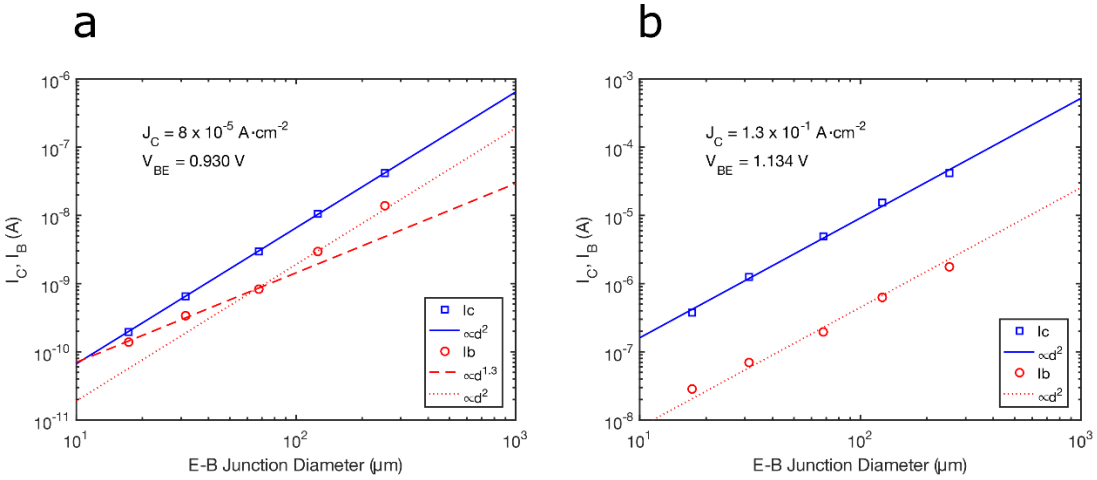

Figure 6: Collector current and base current vs device size (emitter-base junction diameter) for $GaAs_{0.825}P$ HBT. Plotted at low (a) and high (b) current densities. Trend lines are plotted with the approximate slopes noted in the legend.

3.3 Collector Current Behavior

The collector current of GaAs/InGaP HBTs has been previously modelled as thermionic emission of electrons from the emitter into the base, due to the sharp peak in the conduction band created by the abrupt emitter-base junction.[2] These injected electrons diffuse across the base, combining only slightly with majority holes, into the collector. Therefore, collector current can be written as:

$$I_C = A_E A^* T^2 \exp\left(-\frac{E_A}{kT}\right), \quad (1)$$

where A_E is the area of the emitter-base junction, $A^* = 4\pi q m_e^* k^2/h^3$ is the effective Richardson constant for thermionic emission and E_A is the activation energy for injected electrons—the difference between the Fermi level in the emitter and the top of the conduction band peak at the emitter-base interface. Equation 1 can also be extended to the GaAsP/InGaP system. As in Kobayashi, et al., the conduction band offset (ΔE_C) can be written in terms of known quantities:

$$\Delta E_C = nkT\ln\left(\frac{A^* T^2}{I_C}\right) + (1-n)\delta_1 + \delta_2 + qV_{BE} - E_{g,B} \quad (2)$$

where $E_{g,B}$ is the band gap of the base, V_{BE} is the base-emitter voltage, δ_1 is the energy difference between the Fermi level and conduction band edge in the neutral emitter, and δ_2 is the energy difference between the Fermi level and the valence band edge in the neutral base. n, the collector current ideality factor, can be measured directly from the I_C vs V_{BE} curve. δ_1 and δ_2 are not ignored in Equation 2 because unlike in Kobayashi, et al., the dopant concentrations of the emitter and base are such that they are non-negligible. $E_{g,B}$ values can be obtained from the PL data in Figure 2 as described in Section 3.1. m_e^* values for InGaP can be linearly interpolated between $0.15m_0$ for GaP (Γ valley) and $0.08m_0$ for InP, and m_h^* values for GaAsP can be linearly interpolated between $0.79m_0$ for GaP and $0.51m_0$ for GaAs. Therefore, all values on the right-hand side of Equation 2 are known.

If Equation 2 is used to calculate ΔE_C for the GaAsP/InGaP HBTs presented here, negative values ranging from –20 to –40 meV are yielded. This is true for any I_C - V_{BE} pair from the $n \approx 1$ regime. Of course, a negative or even a sufficiently small positive value of ΔE_C means that the above model of thermionic emission does not apply. Kobayashi, et al. report a ΔE_C of 30 meV

for the InGaP/GaAs heterojunction according to the thermionic emission model. The discrepancy between their result and ours (for the GaAs/InGaP device) is due to one of two possibilities. First, the InGaP emitter in this work was grown at a temperature of 650 °C, while in Kobayashi, et al., it was grown at 700 °C. Evidence of Cu-Pt ordering in the emitter regions of the device can be seen in Figure 3b. Cu-Pt ordering occurs in InGaP grown at temperatures between around 550 °C and 750 °C with a corresponding reduction in band gap that is greatest near 650 °C.[20] The shift in band gap would therefore be greater for our GaAs/InGaP sample than for Kobayashi, et al., resulting in a smaller conduction band offset. Second, because our samples have a lower base doping than those in Kobayashi, et al., the depletion width of the emitter-base junction extends further into the base. This reduces the prominence of the conduction band peak at the emitter-base interface.

In either case, it can be concluded that thermionic emission from the InGaP emitter into the GaAsP base due to the conduction band offset does not significantly affect I_C. This can be confirmed by comparing I_C in the forward-active regime (FAR) with the emitter current (I_E) in the reverse-active regime (RAR). In RAR, I_E is a measure of electrons injected from the collector into the base. Because the collector and base are the same material, there is no conduction band offset at the base-collector junction. In Figure 7, I_C in FAR and I_E in RAR are compared for GaAs/InGaP and $GaAs_{0.825}P$/InGaP HBTs, both with emitter-base junction diameters of 60 μm. The ideality factors for both FAR and RAR are n = 1.02 for the GaAs/InGaP device and n = 1.06 for the $GaAs_{0.82}P$/InGaP device. This demonstrates that in both modes of operation, carrier transport is limited by diffusion across the base layer, not by the conduction band offset. The ideality factor would be expected to be significantly higher in FAR than in RAR if it was limited by thermionic emission across the emitter-base junction.[21]

Therefore, I_C can be modeled solely by diffusion of electrons across the quasi-neutral base layer, which can be written as:

$$I_C = A_E \frac{qD_{n,B}}{X_B} \frac{n_{i,B}^2}{N_B} \exp\left(\frac{qV_{BE}}{kT}\right), \tag{3}$$

where $D_{n,B}$ is the diffusivity of electrons in the base, X_B is the quasi-neutral base thickness, $n_{i,B}$ is the intrinsic carrier concentration in the base, N_B is the p-type doping level in the base.[22] Figure 8 shows I_C predicted by this diffusion process along with the measured I_C for the GaAsP HBTs of different composition, all at V_{BE} = 0.9 V and V_{BC} = 0 V. For the GaAs device (x = 1), the measured I_C is well-predicted by this model to within the expected error. However, for all of the GaAsP devices (x < 1), the measured I_C is about 10 times higher than what is predicted. The origin of this behavior is unknown and under further investigation, but a higher I_C for a given V_{BE} is beneficial because it yields a higher transconductance.

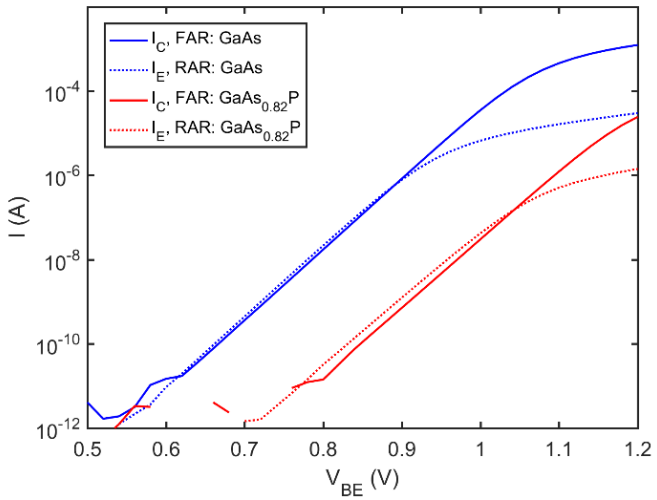

Figure 7: Collector current in the forward-active regime (FAR) and emitter current in the reverse-active regime (RAR) for GaAs/InGaP and $GaAs_{0.82}P$/InGaP HBTs. The emitter-base junction diameter is 60 μm.

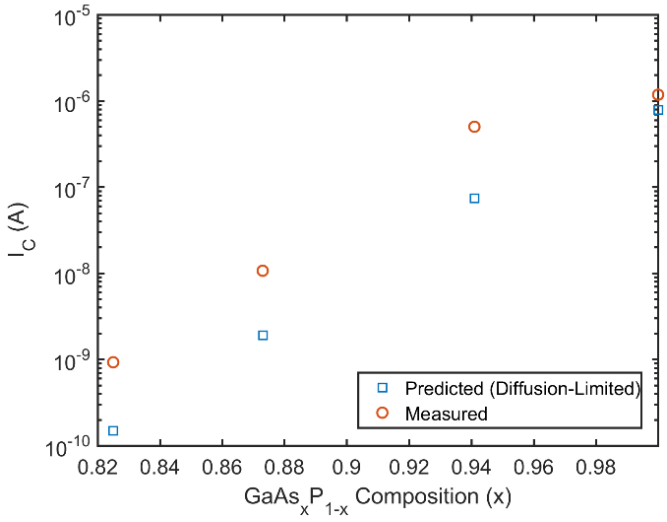

Figure 8: Predicted and measured collector current for V_{BE} = 0.9 V and V_{BC} = 0 V. Emitter-base junction diameter is 60 μm.

4 Conclusions

This paper demonstrates the DC performance of $GaAs_xP_{1-x}/In_yGa_{1-y}P$ HBTs of multiple compositions (ranging from x = 0.825 to x = 1) grown on GaAs substrates. DC current gain nearing 100 is measured for 60 μm diameter devices of each composition, and is shown not to vary significantly as a function of composition for a given I_C. Mechanisms behind I_B are identified for different regimes. For low current densities and smaller device sizes, I_B is caused by SCR recombination at the perimeter of the device. For higher current densities and larger device sizes, I_B is caused by a combination of QNR and SCR recombination across the entire area of the emitter-base junction. I_C is shown not to be limited by thermionic emission over a barrier formed by the conduction band discontinuity between the InGaP emitter and the GaAsP base. Modeling I_C as diffusion of electrons across the quasi-neutral base agrees well with measurements for the GaAs/InGaP HBT, but underestimates measured I_C for all GaAsP/InGaP devices by almost 10 times. Features such as higher transconductance and more convenient

lattice constants portend GaAsP/InGaP HBTs as candidates for integration into silicon CMOS platforms.

5 Acknowledgements

This work was supported by the Center for Energy Efficient Electronics Science (NSF Award 0939514). This work made use of the MRSEC Shared Experimental Facilities at MIT, supported by NSF Award DMR-14-19807. Device fabrication was performed at MIT's Microsystems Technology Laboratory. The authors would like to thank Rushabh Shah and Roger Jia for their helpful input.

References

[1] F.H. Chau, B.J. Lin, Y. Chen, M. Kretschmar, C. Lee, N.L. Wang, X. Sun, W. Ma, S. Xu, and P. Hu, 191 (2006).

[2] T. Kobayashi, K. Taira, F. Nakamura, and H. Kawai, J. Appl. Phys. **65**, 4898 (1989).

[3] C.R. Abernathy, F. Ren, P.W. Wisk, S.J. Pearton, and R. Esagui, Appl. Phys. Lett. **61**, 1092 (1992).

[4] J.J. Tietjen and L.R. Weisberg, Appl. Phys. Lett. **7**, 261 (1965).

[5] E. Fitzgerald, M.T. Bulsara, Y. Bai, C. Cheng, W.K. Liu, D. Lubyshev, J. Fastenau, Y. Wu, M. Urtega, W. Ha, J. Bergman, B. Briar, C. Drazek, N. Daval, F. Letertre, W.E. Hoke, J.R. LaRoche, K.J. Herrick, and T.E. Kazior, ECS Trans. **19**, 345 (2009).

[6] W.E. Hoke, R. V. Chelakara, J.P. Bettencourt, T.E. Kazior, J.R. LaRoche, T.D. Kennedy, J.J. Mosca, a. Torabi, a. J. Kerr, H.-S. Lee, and T. Palacios, J. Vac. Sci. Technol. B Microelectron.

Nanom. Struct. **30**, 02B101 (2012).

[7] K.H. Lee, S. Bao, E. Fitzgerald, and C.S. Tan, Jpn. J. Appl. Phys. **54**, 1 (2015).

[8] V.K. Yang, M. Groenert, C.W. Leitz, A.J. Pitera, M.T. Currie, and E.A. Fitzgerald, J. Appl. Phys. **93**, 3859 (2003).

[9] S.M. Ting and E.A. Fitzgerald, J. Appl. Phys. **87**, 2618 (2000).

[10] M.J. Mori, S.T. Boles, and E.A. Fitzgerald, J. Vac. Sci. Technol. A Vacuum, Surfaces, Film. **28**, 182 (2010).

[11] S. Tomasulo, K.N. Yaung, and M.L. Lee, IEEE J. Photovoltaics **2**, 56 (2012).

[12] E.A. Fitzgerald, A.Y. Kim, M.T. Currie, T.A. Langdo, G. Taraschi, and M.T. Bulsara, Mater. Sci. Eng. B **B67**, 53 (1999).

[13] C. Heidelberger and E.A. Fitzgerald, J. Cryst. Growth **446**, 7 (2016).

[14] W.S. Hobson, Y.K. Chen, and M.C. Wu, Semicond. Sci. Technol. **7**, 1425 (1992).

[15] M. Razeghi, F. Omnes, P. Maurel, Y.J. Chan, and D. Pavlidis, Semicond. Sci. Technol. **6**, 103 (1991).

[16] V. Swaminathan and A.T. Macrander, *Materials Aspects of GaAs and InP Based Structures* (Prentice-Hall, Inc., 1991).

[17] C.L. Andre, M. Gonzalez, M.K. Hudait, E.A. Fitzgerald, J.A. Carlin, M.T. Currie, C.W. Leitz, T.A. Langdo, E.B. Clark, D.M. Wilt, and S.A. Ringel, Photovolt. Spec. Conf. 1043 (2002).

[18] R.A. Bruce and G.R. Piercy, Solid. State. Electron. **30**, 729 (1987).

[19] S. Tiwari and D.J. Frank, Appl. Phys. Lett. **60**, 630 (1992).

[20] T. Suzuki, A. Gomyo, S. Iijima, K. Kobayashi, S. Kawata, I. Hino, and T. Yuasa, Jpn. J. Appl. Phys. **27**, 2098 (1988).

[21] J.S. Yuan, *SiGe, GaAs, and InP Heterojunction Bipolar Transistors* (John Wiley & Sons, 1999).

[22] W. Liu, *Handbook of III-V Heterojunction Bipolar Transistors* (John Wiley & Sons, 1998).